IEEE TRANSACTIONS ON
ANTENNAS AND PROPAGATION

IEEE Xplore® Digital Library
http://ieeexplore.ieee.org/Xplore

Optically-Upconverted, Spatially-Coherent Phased Array Antenna Feed Networks for Beam-Space MIMO in 5G Cellular Communications

Dennis W. Prather, *Senior Member, IEEE*, Shouyuan Shi, Garrett J. Schneider, Peng Yao, Christopher Schuetz, Janusz Murakowski, Joseph C. Deroba, *Member, IEEE*, Fuquan Wang, Matthew R. Konkol, and Dylan D. Ross

***Abstract*— The densification of cellular networks and their soon- to-increase operational frequency is forcing new topological considerations in 5G networks. In particular, networks that enable extreme spatial discrimination are being considered as a means to significantly increase data capacity by realizing spatial-spectral channels that offer frequency re-use without co-channel or adjacent-channel interference. In this paper, we present a new approach to realizing such a capability based on optically-upconverted, spatially-coherent phased-array feed networks. The details of our approach, presented herein, include the design and initial demonstration of both transmit (Tx) and receive (Rx) array systems that are used in tandem to form a down- / up-link for the purpose of characterizing both array and link performance. Design parameters and initial link characterization results are presented.**

***Index Terms*— current sheet, optically fed phased array networks, tightly coupled arrays**

I. Introduction

With the advent of 5G, the rapid and extensive deployment of wireless communication networks that has occurred over the last few decades is about to undergo a new phase of transformation. In particular, the role of spatial multiplexing will increase significantly with innovations in beam-space MIMO (BS-MIMO) [1]–[4], which provides a significant increase in data volume [5], [6] by creating dense spatial sectors where each corresponds to an independent communication channel, see Fig. 1. In this context, user equipment (UE) within a given sector will not interfere with UEs in adjacent sectors, thereby rendering orthogonal communication channels with each having access to significantly increased spectrum. This arises from the lack of interference, by virtue of spatial isolation, which enables frequency re-use across spatial sectors. In addition, the power within a given sector can be tailored to increase fade margins thereby ensuring robust coverage in interference limited environments, as well as accounting for cell margin fading in a spatially precise and energy-efficient way.

This work was supported in part by the National Science Foundation (Award No. 1509081), U.S. Air Force Research Laboratory and the Air Force Office of Scientific Research.

D. Prather, S. Shi, G. Schneider, J. Murakowski, J. Deroba, F. Wang, M. Konkol, and D. Ross are with the Department of Electrical & Computer Engineering, University of Delaware, Newark, DE 19716, USA (e-mail: dprather@udel.edu, sshi@udel.edu, gschneid@udel.edu, jam@udel.edu, joseph.deroba@gmail.com, fuquan@udel.edu, mrkonkol@udel.edu; ddross@udel.edu;).

C. Schuetz and P. Yao are with Phase Sensitive Innovations, Inc., Newark, DE 19711, USA (e-mail: schuetz@phasesensitiveinc.com; yao@phasesensitiveinc.com).

Digital Object Identifier: 10.1109/TAP.2017.2735549

Accordingly, spatial orthogonalization implies that signals within a given sector are mapped by the transmit (Tx), or receive (Rx), antennas either from, or onto, unique Tx/Rx elements of the base station. In this case, the Tx array will radiate into specific and pre-determined sectors and the Rx array will receive and spatially separate signals from particular spatial sectors. The process of spatially mapping a signal either into, or from, a given sector within the environment is that of beam forming. Mathematically speaking, in the absence of environmental scattering, this process represents a spatial Fourier-transform operation, which can be achieved through digital computation or through spatial imaging. While imaging is ubiquitous within the optics community, in comparison, it is less common within the RF community. That being said, the desire to incorporate spatial multiplexing in 5G networks is renewing interest in beam forming using both techniques [7]–[9].

II. Background

A. Spatial beam forming approaches

Broadly speaking, there are two general approaches to array-based beam forming: digital and analog. In digital beam forming (DBF) [3], [7] an array of RF channels either transmits or receives the desired signal into, or from, a desired sector. On the transmit side, a digital-to-analog converter (DAC) is used to feed an I/Q signal into each channel of the array feed network, which includes oscillators, mixers, high-power-amplifiers (HPAs), filters, and antenna elements. While such feed networks offer significant flexibility in terms of agile beam forming, their efficacy can be degraded by errors induced by less than perfect channel synchronization arising from uncorrelated variations in amplitude and phase of the local oscillators across the array. Such errors can also arise due to non-linearities within the DAC, such as clock-jitter or quantization errors. While using synchronization signals can reduce these errors, this comes with the added complexity of additional signal routing and the need for associated amplifiers, with their own non-linearities, to off-set routing losses. Lastly, inherent non-linearities within the HPA can introduce inter-mixing and intermodulation that can also give rise to increased adjacent channel leakage ratios (ACLRs).

On the receive side of a DBF system RF channels may include multiple low-noise amplifier (LNA) stages, filter(s), oscillator(s), mixer(s) (for down-conversion to an intermediate

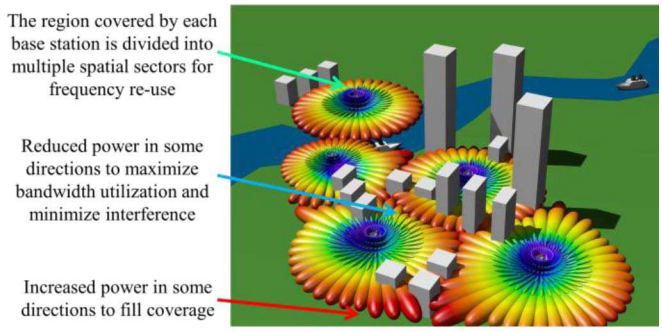

Fig. 1. Spatial channelization by dividing coverage areas into angular sectors where each can operate with little to no interference from adjacent sectors and thereby have full spectrum access, or frequency re-use.

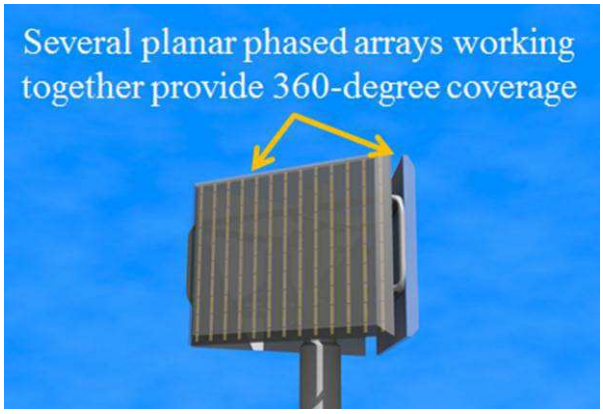

Fig. 2. Depiction of an 'ideal' base station utilizing optically-upconverted phased arrays with analog beam forming for spatial channelization.

frequency (IF)), and an analog-to-digital converter (ADC). Once digitized, all outputs from the RF channels are fed to a digital signal processor (DSP) to render a spatial-spectral map of the cellular environment. With this approach, system performance can be affected by the inherent non-linear properties of the RF front-end, where the individual elements contribute a cascade of 2^{nd} and 3^{rd} order non-linearities that serve to intermix and intermodulate the received signals from every UE in the environment. This can result in frequency spurs that exist both in-band and out-of-band, which ultimately limit the extent to which one can achieve spatial-spectral orthogonality. Additionally, quantization errors that arise in both the DAC and ADC introduce a lower bound on the noise floor within a particular communication channel.

To overcome these limitations, phased-array analog beam combiners can be used, which are feed networks that use phase shifting and transmission-length adjustment to perform spatial beam forming. Such analog beam combiners come with the cost of limiting the number of beams that can be formed simultaneously and a narrowing of the operational bandwidth.

An alternate approach that combines the advantages of DBF and analog beam combiners is to use a lens-based antenna that offers the ability to perform analog beam forming, or imaging. Over the years, there have been various implementations of lensed antennas [8]–[10], using Luneburg [11], [12], Rotman [13], [14], and Zoned lenses [15], within the RF community and more recently in the context of beam-space MIMO applications [16]–[18]. The work presented in Reference [16] uses a Luneburg lens to create spatial sectors within a stadium environment and was shown to provide a substantial increase in data rates both in aggregate and within each spatial sector. In References [17], [18] a flat, zoned lens, based on miniaturized-element frequency-selective surfaces (MEFSSs) to impart the requisite phase profile across the various zones of the lens, was used to demonstrate the ability to realize spatial communication channels.

With the use of lens antennas come practical limitations in terms of deployable systems. In the case of Luneburg lenses, their size and weight, especially at lower frequencies, limits their appeal within the cellular environment. In the case of References [15], [17], [18], there are fundamental limits in diffraction efficiency that arise from the zonal approximation of a continuous lens profile [19]. Such limits on efficiency can give rise to crosstalk between sectors and thereby reduce spatial-spectral orthogonality. Also, in both cases the lens profiles are frequency dependent and, consequently, have limited operational bandwidth, which will limit their use to discrete regions of the spectrum. In addition, when single-lens-based approaches are used, the mapped or imaged signals collect over a focal-arc, or Petzval surface, thereby requiring the receiver array to be fabricated on a non-planar surface. Lastly, lens systems scale in three-dimensions, meaning that as the lens increases in cross-sectional area, which is required to increase the number of orthogonal spatial sectors, the corresponding Rx system increased in volume. This ultimately limits the ability to reduce their form-factor, which can preclude their use in certain locations or environments.

B. Proposed alternative beam forming concept for Rx and Tx

In consideration of the above discussion, a desirable beam forming system for 5G cellular communications would include an analog front-end, such as beam combiner or lens antenna, to minimize quantization errors and non-linearities, but still offer the agile beam forming of DBF along with the form-factor of a phased-array antenna, see Fig. 2.

Our approach to realizing such a system relies on optical up-conversion of RF signals in a spatially coherent phased-array antenna to enable analog beam forming in a planar/conformal array form factor. Key to our approach is the ability to upconvert all transmitted and received RF signals using an analog process that preserves *spatial coherence* across the entire array and over broad bandwidth.

On the receive side, spatial coherence is achieved using a common, or single-laser feed for all channels in the array, with each channel containing an optical modulator connected directly to an antenna element that upconverts the received RF signal right at the RF, or antenna, front-end. At the output of each antenna element is an optical fiber that contains the upconverted RF signal, now a sideband on the optical carrier. This way, the RF wave-front reaching the antenna array is converted to an optical wave-front propagating in an optical-fiber bundle. The fiber outputs are then collected into

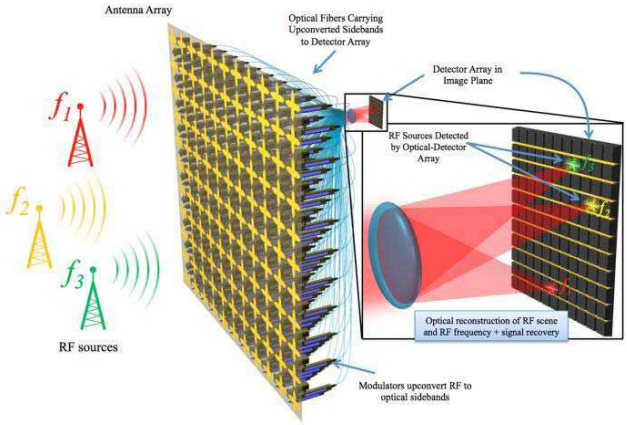

Fig. 3. Illustration of a phased array imaging receiver that performs spatial processing on a large beam-bandwidth-product before signal detection and thereby mitigates signal intermixing and intermodulation.

an array whose layout directly mimics that of the antenna array, albeit at a reduced scale. At this point, the optical sideband containing the RF signal is filtered off the carrier and allowed to propagate in free space. As the filtered output from each fiber expands, the collective overlapping sidebands, which carry the information about the amplitude and phase of every RF signal received by each antenna element, coherently combine to give rise to a spatially-coherent representation of the RF signal, but in the optical domain.

Now that we have a spatially-coherent, upconverted version of the entire RF-signal environment, we can leverage the field of Fourier Optics [20], where a single lens can be used to perform massive spatial processing, namely an analog Fourier Transform, at the speed of light, in parallel, and consuming no power, see Fig. 3. We refer to this approach as an *imaging receiver* and see it as becoming particularly relevant with millimeter-wave bands being made available by the Federal Communications Commission [21].

To our knowledge, the system of Fig. 3 is the first developed RF receiver that first spatially processes all of the received signals using Fourier Optics and, in so doing, spatially maps every received RF signal onto a different/unique photo-detector, which can then be down-converted to an intermediate frequency (IF) or baseband signal and individually processed in the receiver. This *imaging* process serves to mitigate signal intermixing and intermodulation from adjacent sectors as each RF signal within a given sector is imaged onto a unique photo-detector by virtue of the spatial Fourier transform performed by the lens.

It is noted that a feature unique to the proposed approach, in comparison to lens-antenna systems [15], [17], [18], is that it provides the means to encode complex weight profiles across the Rx array aperture thereby enabling the use of a "matched" spatial filter to mitigate multi-path effects and, consequently, account for channel-state information (CSI) in each received signal. Moreover, by using an optical Fourier-transform lens, the spatial processing on the up-converted RF signals, e.g., enhancing the signal-to-interference-ratio (SINR) through spatial correlation, is performed nearly instantaneously, without the use of an analog-to-digital converter and subsequent DSP. This significantly reduces latency and thereby offers the ability to spatially process all received RF signals in the environment in a real-time, optimal way that maximizes utility of the cellular communication infrastructure.

To realize the complementary capability on the transmit side requires commensurate analog (limited only by the DAC feed signal) amplitude and phase control over an ultra-wideband (UWB), low profile RF transmitting antenna. As elemental radiators comprising the phased array antenna impose limitations on array characteristics and performance, the antenna element type selection is key to the aperture design. Efforts to achieve UWB operation have been demonstrated with phased arrays comprised of tapered-slot and bunny-ear antennas [22]–[27]; however, these suffer from profile issues, scan blindness, and complex balun operation. Employing connected dipoles or tightly coupled dipoles in a phased array helps address the first two issues while maintaining UWB operation [28]–[30]. Moreover, these tightly coupled arrays (TCA) of dipoles embody the current sheet array (CSA), which most closely approaches an ideal continuum of amplitude and phase controllable radiating elements [31]–[33]. While such transmission apertures, approximated by tightly coupled dipoles, for RF signals have been a long-sought-after ideal, the dense feed network necessary to drive this antenna array has proved elusive in electronics due to bulky and/or complex impedance matching components.

To address this challenge, we developed an optically-fed TCA concept that enables a close approximation to an ideal current-sheet array antenna, see Fig. 4. In previous work [34]–[38], we introduced such an array that used a coherent optical feed network for analog RF amplitude and phase control as well as high-fidelity RF signal generation at each element in the array. Here, we leverage progress in the development of high-power, high-linearity photo-detectors [39], [40], which have been shown to output RF power of over 1 W at 10 GHz under continuous wave operation and over 10 W peak power at 10 GHz using low duty-cycle pulses [41]. Arrays with up to 24 dBm radiated power per element have also been demonstrated [42]. Power conversion efficiencies of these diodes are also promising, with near 40% having been achieved for direct continuous-wave (CW) RF generation [40], and efficiencies in excess of 50% using modulation formats optimized for use with such devices [43], [44].

We use these detectors to realize a photo-detector coupled-array antenna, which is an approximation to an ideal current sheet array where the current sources exciting the coupled dipole elements are photo-detectors. This antenna design provides maximum relative bandwidth and scanning angle, in addition to being low profile due to the inherent planar dipole structure and ultra-wide operational bandwidth of the CSA. Additionally, the fundamental trait of the TCA that enables its approximation to the ideal CSA is the high degree of element oversampling that, when combined with the small photo-detector die size (0.5 mm $\times$ 0.5 mm), sets the photo-detector bandwidth, which can extend from 500 MHz to 100 GHz, as the upper operational frequency.

To drive the TCA, we developed an optical feed based

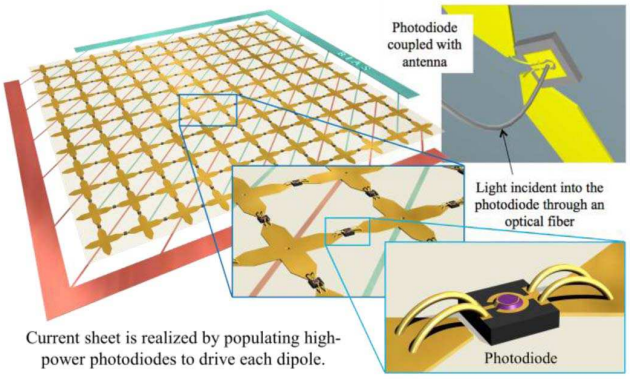

Fig. 4. Illustration of an optically-fed tightly coupled antenna (TCA) phased array that is an approximate implementation of a current-sheet antenna concept.

on two phase-locked lasers that are offset in frequency. The difference frequency is the RF carrier to be transmitted by the array, and because the two lasers are phase-locked the optical phase noise cancels, which results in high-fidelity RF signal generation down to 1-Hz line-width [34]. In this setup, the combined output of the phase-locked lasers is split into N fibers with each fiber being routed to a unique photo-detector, which is directly connected to the feed points of a given antenna element in the TCA, see Fig. 5. Shifting the phase of one laser relative to the other imposes a commensurate phase shift on the RF signal generated by the optical down-conversion on the photo-detector. Likewise, modulating the amplitude of the optical feed yields a commensurate amplitude modulation of the transmitted RF wave. As a result, analog RF beam forming across the TCA is achieved. This approach can realize very complex waveforms that contain extremely high data rates, at well over 1 Gb/s. Moreover, the modulation can be applied to multiple RF carriers in parallel, with simultaneous beam forming that incorporates CSI, thereby realizing a truly complex transmission profile that accounts for the unique aspects of the scattering characteristics of the communication environment. We should also point out that in contrast to lens antennas, if a single photo-detector or even a cluster of photo-detectors were to fail, there is no corresponding loss of a spatial channel; rather, there is only a slight degradation in total radiated power.

An important concern when considering optical signal generation in 5G networking is power efficiency. The generation of optical power via lasers and/or optical amplifiers can be inefficient compared to electronic systems. This issue is mitigated, however, by the ability to convey optical signals over long distances with negligible loss via optical fiber. Hence, high optical power need not be generated at the Tx antenna; rather, it can happen on the ground where power access is not an issue and maintenance costs are low. At the antenna elements, the dissipation in photodiodes should be reasonable. For example, the theoretical limit for photodiodes is 50% efficiency (radiated power per total power dissipated). For a reasonable Tx power per element of 1 W, and an element spacing of 5 mm in a 2-dimensional array (half-wavelength at 30 GHz), this yields a power dissipation requirement of 8 W/cm^2. This is comparable to the typical dissipation of power amplifiers, and furthermore the die sizes of photodiodes and PAs are also comparable. For this reason we are confident that thermal dissipation at the antenna can be managed with simple convective cooling.

In both Tx and Rx, the unique aspect of our approach is that we use optical "up-conversion" to allow for coherent, spatial processing of complex RF signals over the entire array-antenna aperture. Perhaps a main advantage of this approach is that it allows for the spatial processing of all the RF waves in the communication environment prior to actual signal transmission or detection, which mitigates their collective interaction and intermixing. Ultimately, such spatial multiplexing enables frequency re-use on a massive scale as each sector can have access to the entire spectral band while preserving signal integrity through spatial orthogonality between sectors.

In the sections below, we present an overview of the Tx and Rx arrays and their associated optical-feed networks, as well as their demonstration in forming an up- / down-link for characterization of phased array and system performance.

III. Optically-Fed Phased Antenna Arrays

A. Tx Array Optical Feeding Approach

As discussed above, the system concept for the optically-fed Tx beam forming network is shown in Fig. 5, where we have designed an optical network consisting of two correlated laser signals operating at different frequencies ω_1 and ω_2, separated by the desired RF frequency, i.e., $\omega_1 - \omega_2$. These two semiconductor lasers are phase-locked using an injection seeding process that injects a version of the seed laser, shifted in frequency by an amount required for the desired RF frequency offset, into the second laser which maintains optical correlation between the two offset optical beams [34]. By thus establishing temporal coherence, we can ensure that when the two lasers are mixed on the photo-detector, all optical contributions to the phase noise cancel out, as shown in Fig. 6. For this reason, ordinary and inexpensive semiconductor lasers can be used to optically generate high-fidelity RF signals down to 1-Hz resolution, where the phase noise in the generated signal comes only from the RF seed signal that drives the modulator, as shown in Fig. 6(b). Note that the RF seed signal power does not directly control the output power emitted by the photodiodes; rather it provides a phase reference to establish coherence between the lasers, whose optical powers determine the corresponding RF output power. It is also important to note that a unique capability of the system is the distribution of phase-locked, or synchronized, signals across the array thereby alleviating de-synchronization errors arising from uncorrelated oscillators and mixers in digital phased arrays. In addition, the proposed system can be reduced from the use of discrete components in its current realization to photonic integrated circuits (PICs) for a further reduction in size, weight, power, cost and susceptibility to environmental conditions.

Once generated, the phase-locked signals are combined into a single polarization-maintaining (PM) fiber, with the two lasers carried in separate polarization modes. Next, the com-

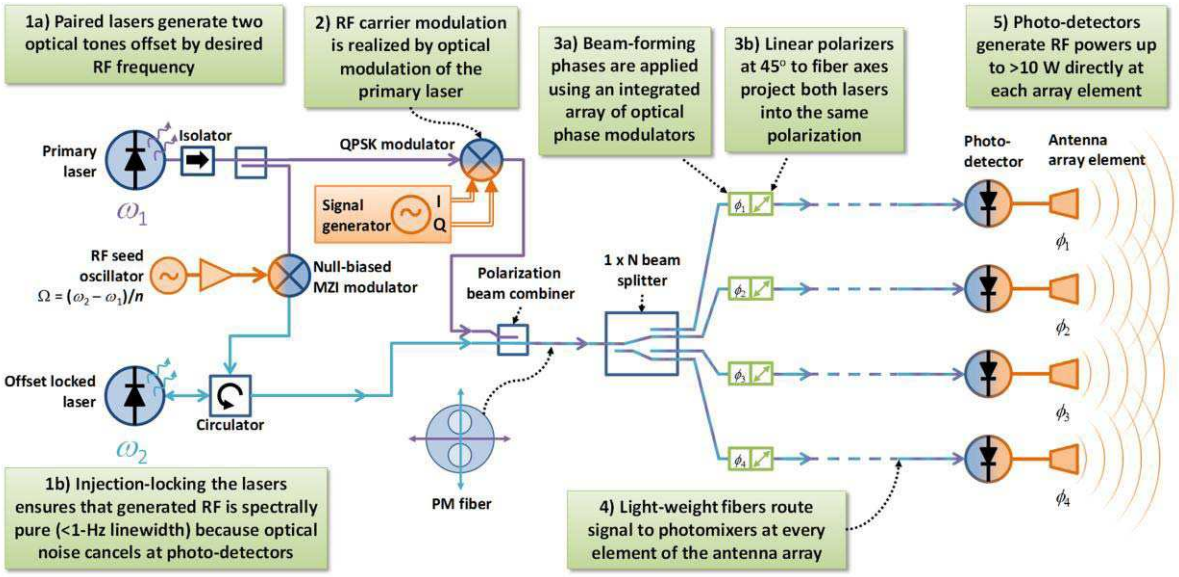

Fig. 5. Schematic layout of an optically-fed phased array antenna network for analog beam forming on a Tx array.

bined fiber is split into M channels followed by analog phase shifters [36], as shown in Fig. 5. The shifters are realized using an integrated array of lithium niobate ($LiNbO_3$) modulators, which have optical insertion loss of 2.2-2.8 dB, and net phase slope of 17°/V, providing resolution of 5×10^{-3} degrees when using a 16-bit, ±10-V DAC (National Instruments 9264). In the phase shifters, the slow and fast axes of the input fiber are aligned, respectively, with the transverse-magnetic (TM) mode (laser 1) and the transverse-electric (TE) mode (laser 2) of the modulator waveguide. If a voltage is applied across the coplanar electrodes, electro-optic modulation is achieved in both polarizations of the optical modes with EO coefficients of r_{33} and r_{13}, respectively [45]. However, since for $LiNbO_3$ $r_{33} = 3r_{13}$, a net phase difference is obtained between the two optical modes. Note that because the phase shifters operate in the optical domain, where a π phase shift corresponds to a propagation delay of just 2.6 fs, significant phase offsets can be applied while imparting negligible delays to the RF signals. After phase modulation, both signals are projected onto the fast and slow axes by applying a 45° rotational key. A linear polarizer is used to filter the two orthogonal signals before they are delivered to each photo-detector, through a single-mode optical fiber. Finally, the signals are fed into each array element with encoded data signals for each UE in the cellular network. We should also point out that a rotation other than 45° will result in an amplitude modulation and thereby provide for a fully complex, analog amplitude and phased modulation profile.

This approach offers several technical and practical advantages over other phased array feed networks including: (1) low-loss transmission; (2) minimum phase noise; (3) light weight, conformal, and flexible distribution to form a 2D array; (4) ultra-wideband operation; (5) no de-synchronization errors across the array arising from uncorrelated oscillators and mixers within each RF channel; and (6) large-scale 2D implementation. These unique characteristics provide a path toward the development of next-generation optically-addressed phased arrays for 5G cellular networks that will allow for a single Tx-array feed network to work at both legacy cellular frequencies (800 MHz–2.4 GHz), as well as, in the emerging millimeter-wave bands [21].

In the section below, we present the use of the proposed beam-forming network as part of a 1×8 tightly-coupled-array as the Tx phased array antenna in a BS-MIMO system.

B. Fabricated Optically-Fed 1x8 Tx Phased Array Antenna

To realize a functional communication channel, we used the above optical feed network to build a 1x8 Tx system for use in a down-link configuration. To this end, we built a 1x8 Tx array antenna, that consisted of the high-power photo-detectors, mounted at the array element feed points, and the optical feed network described above, which is shown in Fig. 7(a). In the design process, we arbitrarily targeted an operational frequency range of 5-20 GHz, providing ultra-wide 4:1 bandwidth while remaining accessible to our test equipment. As Fig. 7(b) indicates, a larger array would extend the bandwidth at the low end, while the high end is limited by the photodiode as described earlier.

To achieve a low profile antenna aperture, we developed a horizontal feed technique that uses a 90° bend enabled by a 2-mm right-angled prism and a GRIN lens assembly to control focal distance/responsivity. In this particular array, all eight photo-detectors were aligned to half responsivity, or roughly 0.3 A/W, to provide adequate output power and ensuring preservation of the photo-detectors. The array is shown in Fig. 7 along with the measured response and output powers of the photo-detectors. More details on the array integration are presented in Ref. [42]. The RF power output of the array is limited by the amount of optical power on the photo-detector and, for the demonstrated array, the effective radiated power was determined using a separate receiver and Friis equation,

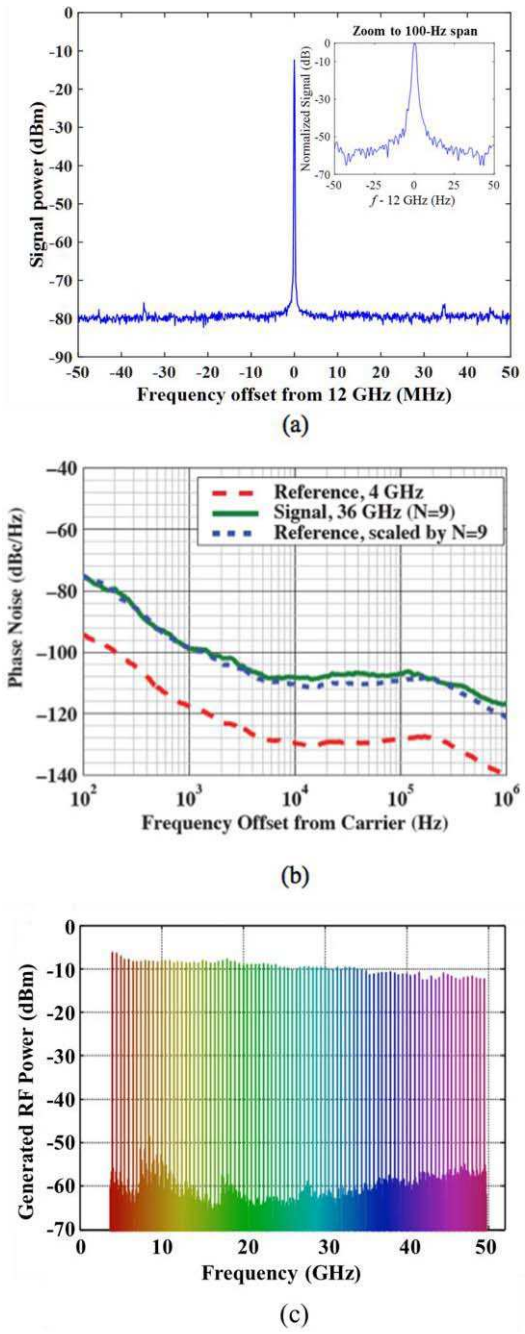

Fig. 6. Characterization data from experimental demonstration of a photonic frequency conversion system [34]. (a) RF spectrum from mixing the master and LO lasers at 12-GHz offset: line-width ∼1 Hz, sidebands ∼ −50 dBc, (b) Phase noise measurements for characterizing coherence between primary and LO lasers, 36-GHz offset, generated from a 4-GHz reference. (c) Spectrum plots showing tuning over a frequency range of 4–50 GHz.

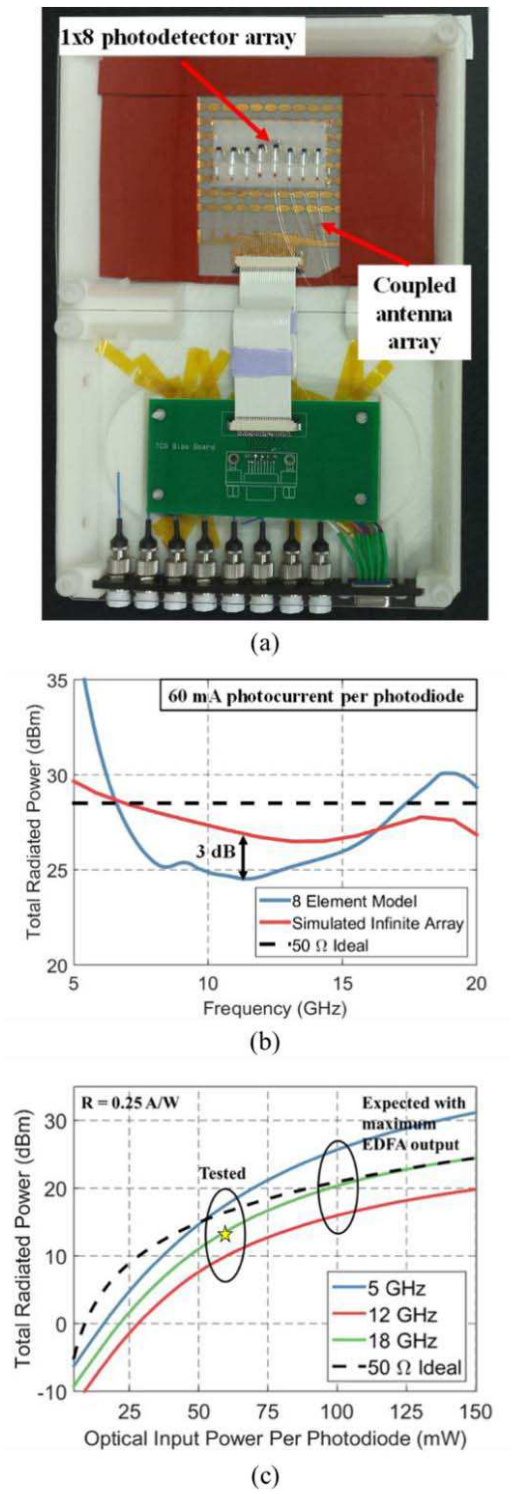

Fig. 7. (a) Fabricated 1×8 optically-fed phased-array Tx antenna, (b) simulations of the total radiated power from the 1×8 array versus frequency using both finite and infinite array models and (c) RF output power per photo-detector versus optical input power.

which compensated for the gain of the receiving antenna and free space path loss. As shown in Fig. 7(c), the measured power at 60 mW optical input power per channel matched well against the expected value at 18 GHz. Despite expectations that the feed network could provide up to 100 mW optical power per photo-detector, the highest observed EIRP was 15 dBm at 17 GHz and 100 mA total photocurrent.

Figure 8 depicts simulated and measured Tx far-field E-plane beam patterns for this array. To obtain these measurements, the array was mounted on a rotation stage and was excited by offset lasers locked at a difference in frequency of 15.94 GHz. The power received at an antenna 2.2 meters from the array was recorded as the array was rotated. The width of the main lobe is 19° , with close agreement between

the simulated and measured results. The asymmetry in the side lobes of the measured beam can be attributed to variations in the RF power transmitted by the 8 elements, which in turn may arise from inconsistencies in the various parameters of the integration process, e.g. the optical alignment of the fibers to the photo-detectors, or the optical power incident on the detectors, or the impedance of the antenna elements.

In the next section, we discuss the design and fabrication of the corresponding Rx array.

C. Optically-Upconverted Rx Phased Array Receiver

On the receive side, we designed and built an Rx system whose front end consists of a 1x8 array of ultra-wideband Vivaldi antennas, with an operational bandwidth of 2-20 GHz, as shown in Fig. 9. At each antenna feed there is a low noise amplifier (LNA) whose outputs are connected to optical modulators. Note that the use of individual Vivaldi antennas merely provides the desired bandwidth for an initial demonstration of our system architecture, which is built around commercial, separately packaged components. Eventually, we plan to integrate LNAs and optical modulators at the feed points of small, dense, tightly coupled antenna elements, as in the Tx TCA concept discussed previously (Fig. 4). The modulators are integrated Mach-Zehnder Interferometer (MZI) modulators that have >30 GHz analog bandwidth and offer high carrier extinction of $\sim$30 dB when properly biased. (Carrier extinction in the modulator reduces optical noise and enables the system to operate more effectively, particularly for lower frequencies where carrier suppression using optical filters is not feasible. Low-frequency operation affords the opportunity to incorporate the frequencies (800 MHz to 2.4 GHz) of legacy networks as well as emerging millimeter-wave frequencies within the same feed network.) The conversion gain in these modulators is typically $\sim$1 W^{-1}, indicating unity power conversion from RF input to optical sideband power when the optical input power is 1 W. Note however, that the optical power is usually less than 100 mW. The LNA gain prior to the modulator is 33 dB, which is required to compensate for the high noise figure of the photonic upconversion, which is presently $\sim$35 dB, but decreases with increasing number of receive channels. Such high LNA gain limits the input saturation power, but this will be mitigated in future implementations by higher channel counts. Further, in the imaging receiver, saturation due to a high-power emitter that is spatially separated from a weak emitter produces spurs that are separated both spectrally and spatially from true signals, improving the system's effective spur-free dynamic range.

After modulation, the upconverted signals are conveyed through optical fibers, which are lightweight, low-loss and have been precisely measured and spliced to match the total path lengths in all 8 channels. Such accuracy is required for the receiver to operate simultaneously over its entire BW; optical phase biases can compensate for variable paths in a narrowband receiver, but length variations result in fixed time delays, thus corresponding to different phase offsets for different frequencies.

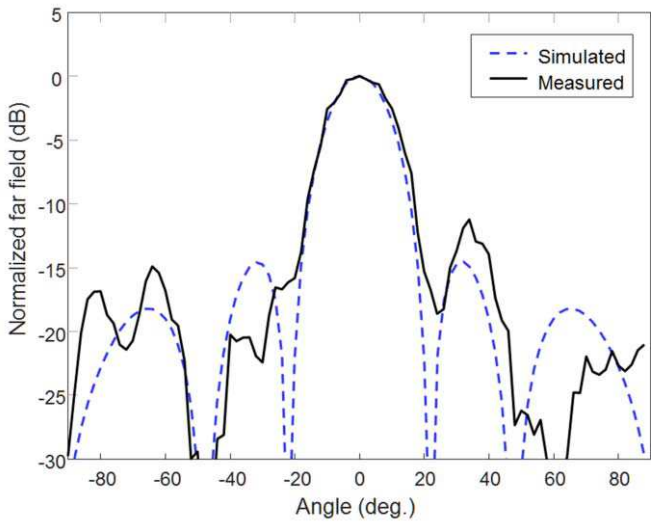

Fig. 8. Tx array E-plane far-field radiation pattern. Both simulation (dashed trace) and measured (solid trace) are shown.

Subsequent to the optical fibers, the signals pass through a 1×8 array of low-speed optical phase modulators that was custom fabricated on a single $LiNbO_3$ PIC. This modulator array is used to apply phase biases to the channels individually, as well as to compensate in real-time for the random phase variations induced by acoustic, mechanical and thermal perturbations of the loose optical fibers. The means of detecting and correcting for these phase variations is implemented as part a free-space optical processor. The modulator array output fibers are connected to the final fiber-based component of the signal chain, an 8-element linear array of polished fibers mounted in a fixed array of grooves patterned in silicon, a so-called V-groove array. The fibers are arranged in the V-groove array such that their positions correspond one-to-one to the positions of the antennas in the antenna array, replicating their spatial positions at reduced scale. In this manner the sideband light emerging from the fiber array replicates the RF field at the antenna aperture, scaled up in frequency, down in size.

From the output facets of the V-groove array, the optical signals emerge into the free-space optical processor. There, additional carrier suppression is achieved by the use of optical bandpass filters; in addition, the reflected carrier light is directed via a polarizing beam splitter into a lens that generates an image of the fiber array, magnified such that each fiber is imaged onto a separate photo-detector in a commercial linear array (Hamamatsu G12430-046D).

The respective image of each fiber is overlaid with a large collimated spot derived from the same laser that feeds the up-conversion modulators. Being from the same laser and arriving at the linear photo-detector array after traveling through a closely matched length of optical fiber, this laser mixes with the focused spots from the rejected carrier light in each fiber, with each photo-detector capturing the beat between each separate signal channel and the common reference. The outputs of these photo-detectors are used to measure and compensate for mechanical/acoustic ($<$20 kHz) phase variations within

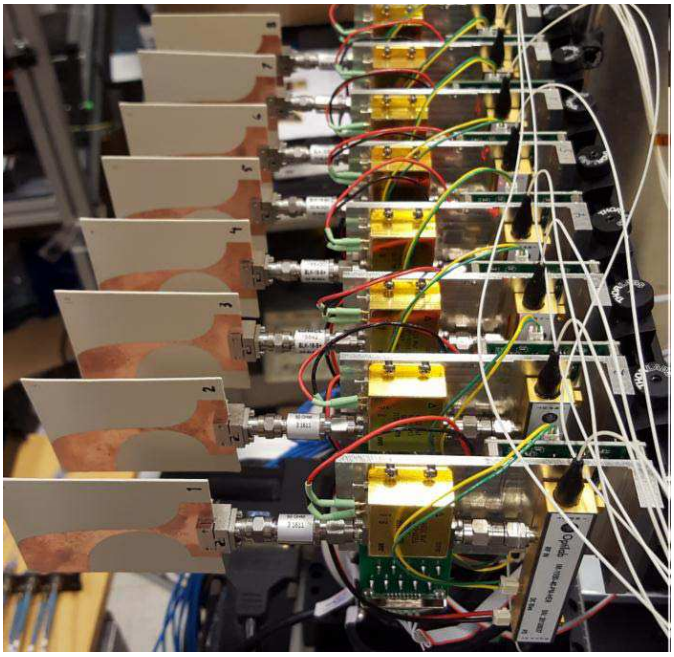

Fig. 9. Photograph of the 1×8 Imaging Receiver system's RF front end, consisting of an array of Vivaldi antennas feeding optical upconversion modulators.

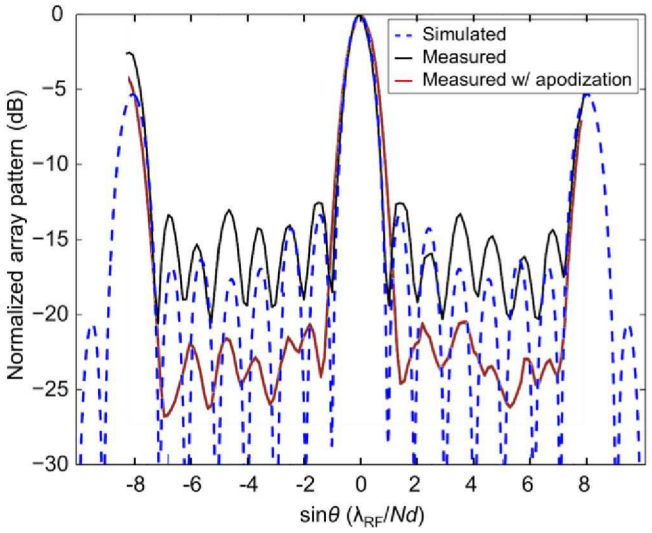

Fig. 10. Simulated (dashed) and measured (solid) optical point spread functions (PSFs) obtained for the 8-channel Rx array, showing the effect of the apodized amplitude profile of Ref. [46] on the sidelobe level. By reciprocity, the optical PSF is a replica of the array's radiation pattern. θ is the angle of incidence, λ_{RF} is the RF wavelength, N is the number of elements in the array, and d is the element spacing ($N = 8$ and d = 3.5 cm, respectively, for the present case).

the fiber feed network in real-time (200-kHz refresh rate) via the 1×8 low-speed modulator array discussed previously. The compensation signals range over 0-40 V, corresponding to a phase tracking range of over 5π radians. They are calculated using an FPGA to reduce latency and free the control computer from the burden of this continuous computation while the system is running. This active-feedback process ensures that the optical signals across the array remain spatially coherent, which allows for the use of Fourier Optics to perform the spatial processing on all of the received RF signals.

After the rejected carriers are used to spatially phase-lock the array, the light from one sideband passes through the optical bandpass filter and continues to propagate into free-space. In so doing, the contributions from each fiber from all the array elements overlap as they propagate and expand in free space. At this point, a lens is used to perform a spatial Fourier transform on the optical field in the lens aperture thereby yielding an image of the sideband energy that replicates the RF scene. Since the imager is 1D, an anamorphic optical system is used to concentrate the energy from the image along the direction transverse to the array. A beam splitter generates two copies of the image plane, wherein two different sensor configurations are used, one optimized for imaging and one for signal recovery. Specifically, the first copy is incident on a camera sensor (New Imaging Technologies WiDy SWIR 320U) that generates an image that can be used to display where RF energy is coming from, i.e., angle of arrival (AoA) or spatial sector, as well as the apparent magnitudes of the imaged sources. The second image copy is formed on another linear photo-detector array (also Hamamatsu G12430-046D). These photo-detectors are read out on a custom circuit board populated with a 2-stage, AC-coupled transimpedance amplifier (TIA) configuration. The TIA provides signal gain and current-to-voltage conversion (5000 V/A), and suppresses output thermal noise. We estimate that the total loss in the path taken by the upconverted signal through optical system is approximately 7 dB, which accounts for both the array gain from coherently combining 7 elements, as well as the combined insertion losses for the various optical components.

The photo-detector bandwidth is insufficient to recover signals at the carrier frequency, hence a coherent tunable optical local oscillator (TOLO) is used to down-convert the sidebands to a suitable IF within the photo-detector bandwidth. It is realized using the same scheme used to produce spectrally pure RF carriers for our Tx system (Fig. 5) [34], except that the offset locked laser is not mixed with the primary laser itself, but rather with the sidebands produced by input RF signals in the Rx upconversion modules. The TOLO output is directed to the optical processor through an optical fiber closely matched in length to the fiber path length of the sidebands, to maximize common-mode rejection of optical noise in the signal recovery. To optimize the alignment of the LO on the photo-detectors, we brought the LO into the optical processor through the same V-groove array that carries the sidebands. This ensures ideal spatial overlap of the signal and LO on the photo-detector, at the expense of the contribution of one channel to the sideband image (hence our 1x8 array has been reduced in practice to a 1×7 array).

The system presently uses a commercial photo-detector array with ∼100 MHz BW, thus we typically use an IF of 60 MHz. Analog waveforms recovered at IF are output from the system via SMA connectors. The eight adjacent photo-detectors can be individually read out simultaneously, with each photo-detector corresponding to a different spatially resolved sector, or direction, in the RF environment. We connect these SMA outputs to an oscilloscope running vector

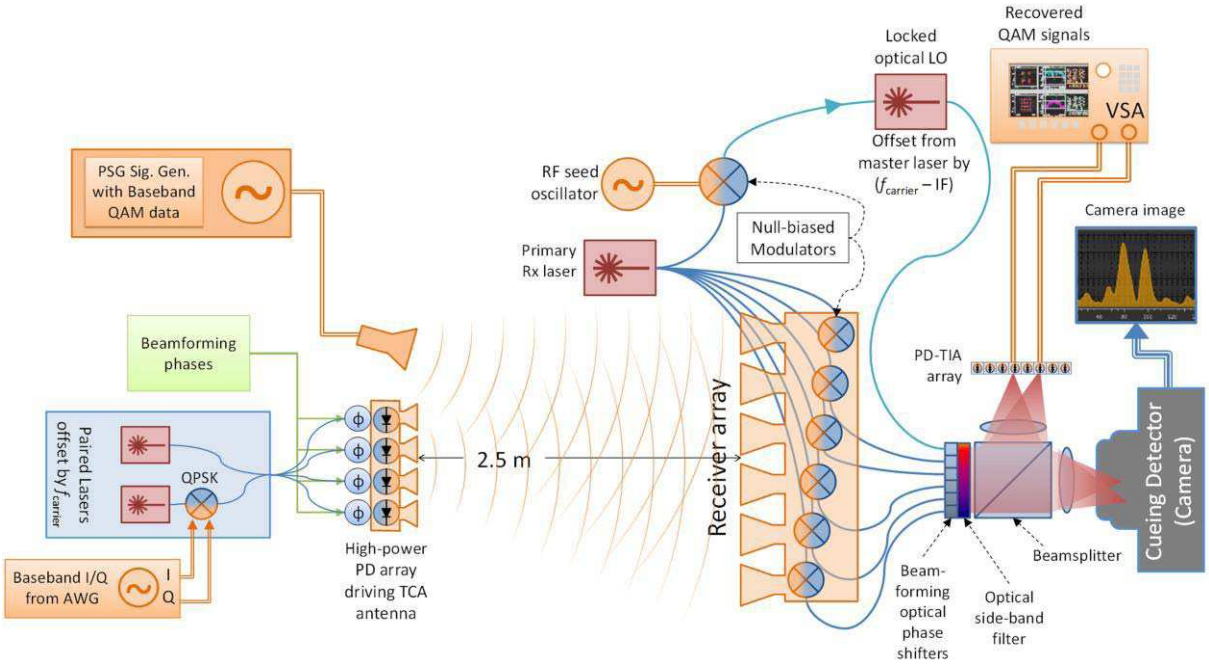

Fig. 11. Schematic layout of the up-/down-link demonstration setup to characterize the performance of the optically-fed Tx and Rx phased-array antennas.

signal analysis (VSA) software to digitize and demodulate the waveforms. The TIA readout board has been designed to suppress oscillations and reduce noise, so that the imaging receiver Rx array is capable of simultaneous high-speed data recovery for all spatial channels.

Due to the small number of elements in the array (only 7 when the optical LO is present), the suppression between co-channel emitters is limited to roughly 12 dB in practice, although this can be improved by carefully adjusting the relative contributions of the channels across the aperture, i.e., by apodization [46]. The effect of apodization can be seen in Fig. 10, which contains images of a point emitter, also called the point spread function (PSF), as captured by the imaging camera, for both flat and apodized amplitude profiles. The sidelobe level is -12 dB without apodization, and improves to -22 dB with it, at the expense of a slight widening of the main lobe. Note that by reciprocity, the PSF of the array is equivalent to the array's radiation pattern. Even though a small level of crosstalk remains, the spatial isolation is sufficient to demonstrate recovery of multiple spatially independent data streams all operating with the exact same carrier frequency, thus, demonstrating frequency re-use. We also should note that a larger and more full, or dense, array can achieve $>$ 40-dB spatial channel isolation. We have measured spur-free dynamic range (SFDR) in the system via 2-tone intermodulation testing, and shown that for emitters in separate spatial sectors, the SFDR is roughly 5 dB improved compared to the case of both tones in the same spatial sector. A larger, more dense array will likewise increase this enhancement.

While the current embodiment of the system allows for signal recovery using a 100-MHz IF bandwidth, we can tune the coherent optical LO that can provide data/signal recovery at any frequency over a 5-20 GHz operational band. The

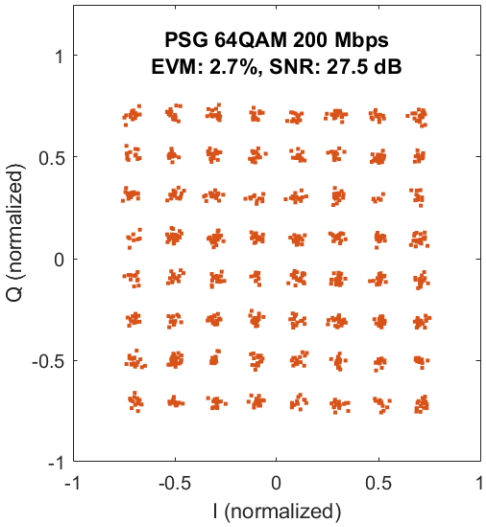

Fig. 12. VSA captured data showing the demodulated 64QAM constellation and spectrum of a signal recovered by the 1x8 Imaging Receiver. This was a 15.94 GHz carrier modulated with 33.33-MSps 64QAM data, for a total data rate of 200 Mbps.

IF is limited by the commercial photo-detectors chosen for expediency. In general, alternate photo-detectors can be used to provide instantaneous bandwidths well over 10 GHz.

IV. Up-/Down-Link Characterization

Figure 11 shows the system configuration used to demonstrate up-/down-link performance. In this configuration two transmitting sources are separated from the imaging receiver Rx array by a distance of 2.5 m. One of the sources on the transmit side consists of an Agilent E8257C PSG with a synthesized signal generator that produced 12dBm of output

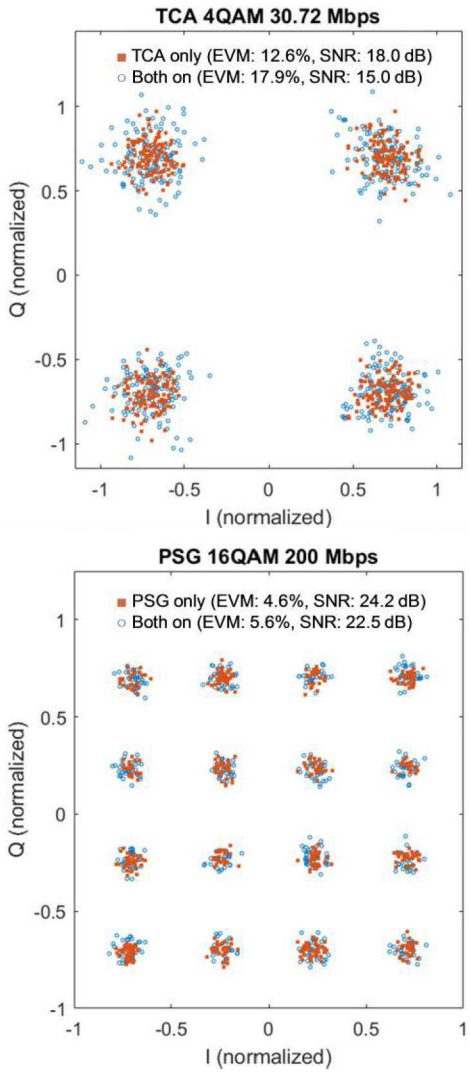

Fig. 13. VSA captured data showing simultaneously demodulated 4QAM (top) and 16QAM (bottom) constellations of signals recovered by the 1x8 Imaging Receiver. This was two 15.94 GHz carriers transmitted simultaneously from locations separated by ∼0.5 m. Data rates of 30.72 Mbps and 200 Mbps were realized and recovered. Plots are shown for both sources when measured separately (red filled markers) and when active simultaneously (blue open markers).

power (including 7 dB of cable loss) at a carrier frequency of 15.94 GHz. The second source was an optically-fed Tx array, where the data signal was a multi-level QAM signal designed by RFXpress software and generated by a 7000 series Tektronix Arbitrary Waveform Generator (AWG) that had a 10 bit DAC and full I/Q modulation. The output of the AWG was fed to an RF-Lambda LNA (R02M04GSA) that had noise figure (NF) of 2.3 dB, a gain of 13 dB and a third-order output intercept point (OIP3) of 38 dBm. The amplified RF signal was input to a Thorlabs LN865-SC QPSK/single sideband modulator, made in $LiNbO_3$. The output from the modulator was combined with the paired laser source and processed by the optical beam-former. The resulting output signals are routed to each of the photo-detectors integrated at the feed-point of each antenna element on the 1×8 array along with their respective optically off-set lasers and phase modulation. Upon down-conversion, each photo-detector had a responsivity of ∼0.33 A/W and generated an output RF power of 10 dBm with 20 mA of current. The paired source was tuned to an off-set of 15.94 GHz and had various levels of QAM, with the resulting data rates presented below.

The first link characterization demonstrated up-link capability, where the PSG was positioned to transmit a beam that aligned with the 6^{th} spatial channel of imaging receiver. In this configuration, the PSG was used to represent a UE in the cellular environment as a means to demonstrate up-link performance. An oscilloscope with VSA software was used to reconstruct the transmitted constellation as spatially processed and recovered from the imaging receiver, as shown in Fig. 12. The data shown depicts a 200 Mbps data stream constellation via 64QAM encoded at 33.33 MSps. The measured EVM and SNR are 2.7% and 27.5 dB, respectively.

The second link characterization demonstrated down-link capability using the Tx array. However, in this setup the PSG was also used to simultaneously transmit a second signal using the exact same carrier frequency as the Tx array. Such simultaneous source and shared frequency transmission demonstrated the ability to have frequency re-use between spatial sectors/channels.

Again, to demodulate and recover the transmitted constellations an oscilloscope with VSA software was used to process the two simultaneous (Tx array (4QAM) and PSG (16QAM)) data streams, which had a common carrier frequency but were modulated with completely independent data rates and modulation formats. As shown in Fig. 13, the output is two simultaneously demodulated 4QAM and 16QAM constellations and spectra of signals recovered by the 1×8 Imaging Receiver. This data consisted of two 15.94 GHz carriers transmitted simultaneously from locations separated by ∼0.5 m and imaged on to the 6^{th} and 8^{th} spatial channels of the imaging receiver. Data rates of 30.72 Mbps and 200 Mbps were realized and recovered. Measured EVM and SNR when both sources were active are: 17.9% and 15.0 dB for the 4QAM signal, and 5.6% and 22.5 dB for the 16QAM signal, respectively.

V. Conclusions

In this paper we presented a set of new optically-upconverted, spatially-coherent phased-array-antenna Tx/Rx feed networks for application to 5G cellular communications. It is based on the application of multiple RF-Photonic devices and subsystems that when integrated represent an imaging receiver as an Rx array and a current-sheet antenna as a Tx array. With the emerging field of photonic integrated circuits and silicon photonics, there is strong potential to integrate the various components on the chip scale thereby reducing cost and increasing reliability.

A unique aspect of this work was in the system-level integration of Tx and Rx optical processors that consists of eight channels for application in the realization of Beamspace MIMO up-/down-link demonstration. In this context, we demonstrated data rates up to 200 Mbps in data transmis-

sion with a signal-to-noise ratio commensurate with error-free transmission. Finally, the developed transmitting phased array and the imaging receiver Rx array antenna have been demonstrated in conjunction to show an end-to-end system demonstration where microwave communications signals have been generated, steered, received, down-converted, and recovered using photonic techniques. Such a system enables a near continuum of spatial-spectral coverage over both legacy and emerging millimeter-wave frequencies.

ACKNOWLEDGMENT

The authors would like to thank the National Science Foundation (Grant No. 1509081), Dr. Robert Nelson, AFRL and Dr. Gernot Pomrenke, AFSOR for their support of this work; Dr. Xiao-Feng Qi and his research team at Futurewei, Inc. for their helpful discussion and guidance in the application of the demonstrated systems to cellular communications; and, Professors Joe Campbell and Andreas Beling of the University of Virginia for valuable discussion and use of their photodiodes.

REFERENCES

[1] L. Fernandes, "Developing a system concept and technologies for mobile broadband communications," *IEEE Pers. Commun.*, vol. 2, no. 1, pp. 54–59, Feb. 1995.

[2] Z. Pi and F. Khan, "An introduction to millimeter-wave mobile broadband systems," *IEEE Commun. Mag.*, vol. 49, no. 6, pp. 101–107, Jun. 2011.

[3] T. S. Rappaport, R. W. Heath, R. C. Daniels, and J. N. Murdock, *Millimeter wave wireless communications*. New York: Prentice Hall, 2015.

[4] K. Maliatsos, P. N. Vasileiou, and A. G. Kanatas, "Performance Evaluation of Beamspace MIMO Systems with Channel Estimation in Realistic Environments," *J. Cyber Secur. Mobil.*, vol. 2, no. 3 & 4, pp. 265–290, Jan. 2014.

[5] D. A. B. Miller, "Spatial channels for communicating with waves between volumes," *Opt. Lett.*, vol. 23, no. 21, pp. 1645–1647, Nov. 1998.

[6] D. A. B. Miller, "Communicating with waves between volumes: evaluating orthogonal spatial channels and limits on coupling strengths," *Appl. Opt.*, vol. 39, no. 11, pp. 1681–1699, Apr. 2000.

[7] Y. T. Lo and S. W. Lee, Eds., *Antenna Handbook: Theory, Applications, and Design*. Springer US, 1988.

[8] P. S. Hall and S. J. Vetterlein, "Review of radio frequency beamforming techniques for scanned and multiple beam antennas," *Antennas Propag. IEE Proc. H - Microw.*, vol. 137, no. 5, pp. 293–303, Oct. 1990.

[9] J. Thornton and K.-C. Huang, *Modern Lens Antennas for Communications Engineering*, vol. 39. John Wiley & Sons, 2013.

[10] J. J. Lee, "Lens Antennas," in *Antenna Handbook*, Y. T. Lo and S. W. Lee, Eds. Springer US, 1988, pp. 1073–1131.

[11] R. K. Luneburg, *Mathematical theory of optics*. University of California Press, 1964.

[12] L. C. Gunderson and G. T. Holmes, "Microwave Luneburg Lens," *Appl. Opt.*, vol. 7, no. 5, pp. 801–804, May 1968.

[13] W. Rotman and P. Franchi, "Cylindrical microwave lens antenna for wideband scanning applications," in *1980 Antennas and Propagation Society International Symposium*, 1980, vol. 18, pp. 564–567.

[14] W. Rotman and R. Turner, "Wide-angle microwave lens for line source applications," *IEEE Trans. Antennas Propag.*, vol. 11, no. 6, pp. 623–632, Nov. 1963.

[15] M. A. Al-Joumayly and N. Behdad, "Wideband Planar Microwave Lenses Using Sub-Wavelength Spatial Phase Shifters," *IEEE Trans. Antennas Propag.*, vol. 59, no. 12, pp. 4542–4552, Dec. 2011.

[16] "AT&T Deploying Giant Ball to Boost Capacity at SXSW," *Wireless Week*, 13-Mar-2015. [Online]. Available: https://www.wirelessweek.com/news/2015/03/t-deploying-giant-ball-boost-capacity-sxsw. [Accessed: 01-Feb-2017].

[17] J. Brady, N. Behdad, and A. M. Sayeed, "Beamspace MIMO for Millimeter-Wave Communications: System Architecture, Modeling, Analysis, and Measurements," *IEEE Trans. Antennas Propag.*, vol. 61, no. 7, pp. 3814–3827, Jul. 2013.

[18] J. Brady, P. Thomas, D. Virgilio, and A. Sayeed, "Beamspace MIMO prototype for low-complexity Gigabit/s wireless communication," in *2014 IEEE 15th International Workshop on Signal Processing Advances in Wireless Communications (SPAWC)*, 2014, pp. 135–139.

[19] D. C. O'Shea, T. . J. Suleski, A. D. Kathman, and D. W. Prather, *Diffractive Optics: Design, Fabrication, and Test*, vol. 62. Washington: SPIE Press, 2004.

[20] J. W. Goodman, *Introduction to Fourier Optics*, 3rd ed. Colorado: Roberts and Company Publishers, 2005.

[21] "FCC Adopts Rules to Facilitate Next Generation Wireless Technologies," *Federal Communications Commission*, 14-Jul-2016. [Online]. Available: https://www.fcc.gov/document/fcc-adopts-rules-facilitate-next-generation-wireless-technologies. [Accessed: 01-Feb-2017].

[22] C. Hemmi, R. T. Dover, F. German, and A. Vespa, "Multifunction wideband array design," *IEEE Trans. Antennas Propag.*, vol. 47, no. 3, pp. 425–431, Mar. 1999.

[23] H. Holter, T.-H. Chio, and D. H. Schaubert, "Experimental results of 144-element dual-polarized endfire tapered-slot phased arrays," *IEEE Trans. Antennas Propag.*, vol. 48, no. 11, pp. 1707–1718, Nov. 2000.

[24] R. W. Kindt and W. R. Pickles, "All-Metal Flared-Notch Array Radiator for Ultrawideband Applications," Sep. 2010.

[25] J. J. Lee *et al.*, "Photonic wideband array antennas," *IEEE Trans. Antennas Propag.*, vol. 43, no. 9, pp. 966–982, Sep. 1995.

[26] J. J. Lee, S. Livingston, and R. Koenig, "A low-profile wide-band (5:1) dual-pol array," *IEEE Antennas Wirel. Propag. Lett.*, vol. 2, no. 1, pp. 46–49, 2003.

[27] J. J. Lee, S. Livingston, and R. Koenig, "Performance of a wideband (3-14 GHz) dual-pol array," in *IEEE Antennas and Propagation Society Symposium, 2004.*, 2004, vol. 1, p. 551–554 Vol.1.

[28] M. Jones and J. Rawnick, "A New Approach to Broadband Array Design using Tightly Coupled Elements," in *MILCOM 2007 - IEEE Military Communications Conference*, 2007, pp. 1–7.

[29] W. F. Moulder, K. Sertel, and J. L. Volakis, "Superstrate-Enhanced Ultrawideband Tightly Coupled Array With Resistive FSS," *IEEE Trans. Antennas Propag.*, vol. 60, no. 9, pp. 4166–4172, Sep. 2012.

[30] E. Yetisir, N. Ghalichechian, and J. L. Volakis, "Ultrawideband Array With 70° Scanning Using FSS Superstrate," *IEEE Trans. Antennas Propag.*, vol. 64, no. 10, pp. 4256–4265, Oct. 2016.

[31] H. Wheeler, "Simple relations derived fom a phased-array antenna made of an infinite current sheet," *IEEE Trans. Antennas Propag.*, vol. 13, no. 4, pp. 506–514, Jul. 1965.

[32] D. Staiman, M. Breese, and W. Patton, "New technique for combining solid-state sources," *IEEE J. Solid-State Circuits*, vol. 3, no. 3, pp. 238–243, Sep. 1968.

[33] B. A. Munk, *Finite Antenna Arrays and FSS*. John Wiley & Sons, 2003.

[34] G. J. Schneider, J. A. Murakowski, C. A. Schuetz, S. Shi, and D. W. Prather, "Radiofrequency signal-generation system with over seven octaves of continuous tuning," *Nat. Photonics*, vol. 7, no. 2, pp. 118–122, Feb. 2013.

[35] J. Bai *et al.*, "Optically Driven Ultrawideband Phased Array With an Optical Interleaving Feed Network," *IEEE Antennas Wirel. Propag. Lett.*, vol. 13, pp. 47–50, 2014.

[36] S. Shi *et al.*, "Conformal Wideband Optically Addressed Transmitting Phased Array With Photonic Receiver," *J. Light. Technol.*, vol. 32, no. 20, pp. 3468–3477, Oct. 2014.

[37] S. Shi *et al.*, "Ultrawideband Optically Fed Tightly Coupled Phased Array," *J. Light. Technol.*, vol. 33, no. 23, pp. 4781–4790, Dec. 2015.

[38] M. R. Konkol *et al.*, "High-power photodiode-integrated connected array antenna," *J. Light. Technol.*, vol. under review, Jan. 2017.

[39] Z. Li *et al.*, "High-power high-linearity flip-chip bonded modified unitraveling carrier photodiode," *Opt. Express*, vol. 19, no. 26, pp. B385–B390, Dec. 2011.

[40] X. Xie *et al.*, "Improved power conversion efficiency in high-performance photodiodes by flip-chip bonding on diamond," *Optica*, vol. 1, no. 6, pp. 429–435, Dec. 2014.

[41] X. Xie *et al.*, "Photonic Generation of High-Power Pulsed Microwave Signals," *J. Light. Technol.*, vol. 33, no. 18, pp. 3808–3814, Sep. 2015.

[42] D. D. Ross *et al.*, "Low-profile, high-power optically addressed phased array antenna," vol. in preparation, 2017.

[43] U. Gliese, K. Colladay, A. S. Hastings, D. A. Tulchinsky, V. J. Urick, and K. J. Williams, "53.5% Photodiode RF Power Conversion Efficiency,"

in *National Fiber Optic Engineers Conference (2010), paper PDPA7*, 2010, p. PDPA7.

[44] U. Gliese, K. Colladay, A. S. Hastings, D. A. Tulchinsky, V. J. Urick, and K. J. Williams, "RF Power Conversion Efficiency of Photodiodes Driven by Mach-Zehnder Modulators," *IEEE Trans. Microw. Theory Tech.*, vol. 58, no. 11, pp. 3359–3371, Nov. 2010.

[45] A. Yariv, *Optical Electronics in Modern Communications*, 5th ed. Oxford University Press, 1997.

[46] J. C. Deroba, G. J. Schneider, C. A. Schuetz, and D. W. Prather, "Smart antenna using element-level photonic up-conversion to generate an apodized beam-space for increased spatial isolation," *IEEE Antennas Wirel. Propag. Lett.*, submitted for review, March 2017.